

## **High-shear granulation: An investigation into the granule consolidation and layering mechanism**

Stefan A. L. de Koster, Kate Pitt, James D. Litster, Rachel M. Smith\*

University of Sheffield, UK

### **Abstract**

The mechanisms of early granule growth are difficult to study and poorly understood. Consolidation and layering play a critical role in the growth process, however little is known about the kinetics.

In this work, a novel consolidation-only granulator (COG) was used to study dynamic consolidation and layering only, eliminating other granulation mechanisms. Prenucleated granule growth was studied over time. Based on experimental data and literature models, a mechanistic layering kernel for population balance modelling was developed.

Granule growth kinetics were qualitatively predicted by a previously reported model; growth behaviour was linear with the square root of time to a certain critical size, after which growth stopped. X-ray computed tomography revealed that consolidation mainly occurred in the outer layers of the granules.

The results greatly advance understanding of consolidation and layered growth, and the new model opens the way for improved predictive modelling and design of granulation processes and products.

## Keywords

Wet granulation; Layering kinetics; Consolidation; Modelling

## 1. Introduction

Granulation is a particle size enlargement technique based on the agglomeration of powder by agitation to form larger agglomerates called granules [1]. Using granulation, the handling, metering and dosing of the materials are improved [2]. One of the methods of achieving this size enlargement is by mixing the powder with a liquid binder. Here, mixing is usually performed in tumbling drums, fluidised beds and high-shear mixers. Due to the many advantages of granulated materials compared to raw powder, granulation is widely applied in many industries, including the pharmaceutical, food, agricultural, detergent and mineral processing industries [3]. Despite the importance of granulation to industry and over 60 years of research [3], wet granulation remains a poorly understood process [4]. This type of granulation involves many different interacting mechanisms, which increase the complexity of the process [4]. In particular, processes involving high-shear mixers are more complex than other methods [5].

Currently, granulation mechanisms are divided into three rate processes [3]. Wetting and nucleation is the formation of initial granules, called *nuclei*. Consolidation and growth describes the densification and growth by layering or coalescence of the nucleated granules. Finally, breakage and attrition involves the destruction and wear of granules. A major breakthrough in the area of granulation came with the introduction of regime maps [6-8] for nucleation and growth. Although these two phenomena are still not fully understood, regime maps have significantly increased our understanding of granulation. However, the mechanisms behind

early stage consolidation and growth, directly after nucleation, have not been fully investigated. In order to model and predict product granule qualities, it is imperative to elucidate consolidation kinetics, as the extent of consolidation determines the porosity and density of granules [1]. These, in turn, determine properties such as strength and friability, dispersion and dissolution; all important critical quality attributes to industrial granulation processes [3]. Furthermore, consolidation determines surface wetness and, therefore, other growth phenomena such as layered growth [1] and growth by coalescence [3].

In the same way that growth is related to consolidation, consolidation is related to nucleation. The current view on nucleation by immersion of powder in droplets considers a powder bed as being static. The droplets spread over the surface of the powder bed and penetrate into the pores, which act as capillaries [3, 9, 10]. The driving force behind this mechanism is surface tension, as described by the Washburn equation [3, 10]. The nucleus then grows by spreading and consolidates by impact and capillary force. This concept also applies to dynamic situations, provided the initial penetration step is fast.

## 1.1. Theory

In the literature, Cameron et al. [11] proposed a method to model layered growth only, which is widely used in population balance modelling (PBM) [11-13]. In the model, the growth rate is described according to Eq (1):

$$G = G_m * \frac{M_{powder}}{k * \sum M_i + M_{powder}} * \exp(-\alpha * (x_w - x_{wc})^2) \quad (1)$$

Here,  $G_m$  is the maximum growth rate,  $M_{powder}$  is the mass of fine powder,  $M_i$  is the mass of particles in size class  $i$ ,  $x_w$  and  $x_{wc}$  are the moisture content and critical moisture content, respectively, and  $k$  and  $\alpha$  are fitting parameters. This model considers the availability of powder as well as the moisture content of the granules, both of which logically affect the growth rate. However, the model contains several empirical parameters, which makes it impossible to predict the layering behaviour of new systems.

Hounslow et al. [14] proposed two more mechanistic 3-D models for consolidation and growth as a result of nucleation. Both models start from a situation in which a droplet of binder is surrounded on all sides by dry powder. This model therefore mostly applies to high-shear mixer granulation, as fluidised bed granulation involves a much more disperse powder. In such processes, the collision frequency between granules and powder play a much more significant role. Terrazas-Velarde et al. [15, 16] performed experimental work to study the kinetics of growth in fluidised bed granulation and developed two models based on physical phenomena. Their first model incorporates interparticle collisions, droplet drying time and liquid addition rate; their second model also takes liquid spreading and penetration into account. These models are not considered in this work, as this work focuses on high-shear mixer granulation.

In Hounslow et al.'s models [14], the granule grows until it has reached a maximum size, which depends on the powder and binder properties. The liquid volume fraction of this final size, which is calculated from the liquid volume divided by the granule volume without air, is called the *critical-packing liquid volume fraction*,  $\phi_{cp}$ .

According to the first model, the nucleus grows in a static environment as a result of surface tension-driven flow. The derived relation shows a linear dependency on the square root of time, as described by Eq (2):

$$\frac{v - v_0}{v_{max} - v_0} = \sqrt{\frac{\gamma * d_p}{18.75 * \mu * h_0^2} * \frac{1 - \phi_{cp}^{1/3}}{\phi_{cp}^3} t} = \sqrt{\frac{t}{t_{max}}} = \sqrt{\tau} \quad (2)$$

where  $v$ ,  $v_0$  and  $v_{max}$  are the volume, initial droplet volume and maximum attainable volume considering the critical-packing liquid volume fraction of the granule, respectively.  $\gamma$  is the liquid surface tension,  $d_p$  is the mean primary particle size,  $\mu$  is the liquid viscosity,  $h_0$  is the initial droplet diameter,  $\phi_{cp}$  is the critical-packing liquid volume fraction and  $t$  is the time after nucleation. The model shows that for a set time,  $t_{max}$ , growth proceeds linearly with the square root of time. After this time has been reached, the granule stops growing.  $\tau$  is the dimensionless time, equal to  $t/t_{max}$ . It should be noted that according to this equation,  $t_{max}$  is dependent on  $\phi_{cp}$ . The second model considers the powder bed as a dynamic medium, and is based on deformation-driven diffusive flow. Small deformations cause migration of liquid and powder, resulting in a ‘diffusion’ of material. The model shows exponential decay of growth, as shown in Eq (3):

$$\frac{v - v_0}{v_{max} - v_0} = 1 - \exp\left(-\frac{12 * D_{eff} * \phi_{cp}^{2/3}}{h_0^2} t\right) = 1 - \exp\left(-12 * \phi_{cp}^{2/3} * \tau\right) \quad (3)$$

Here,  $D_{eff}$  is the effective diffusivity,  $\tau$  is the dimensionless time, defined as  $h_0^2/D_{eff}$ , and the other parameters are the same as in the previous model. This suggested growth behaviour is in

agreement with a model to predict granule porosity over time proposed by Maxim et al. [17]. Their model, which originally uses several different types of interparticle space, may be expressed in terms of  $v$ ,  $v_0$  and  $v_{max}$ , as shown in Eq (4):

$$\frac{v - v_{max}}{v_0 - v_{max}} = \exp(-\omega * t) \quad (4)$$

where  $\omega$  is the agitation rate constant. This model is qualitatively the same as Hounslow et al.'s model [14], although Maxim et al.'s model is based on the agitation rate only, whereas Hounslow et al. created a lumped parameter  $D_{eff}/h_0$  which encompasses all deformation-based interactions. Fig. 1 shows a graphical representation of the behaviour of both of Hounslow et al.'s models.

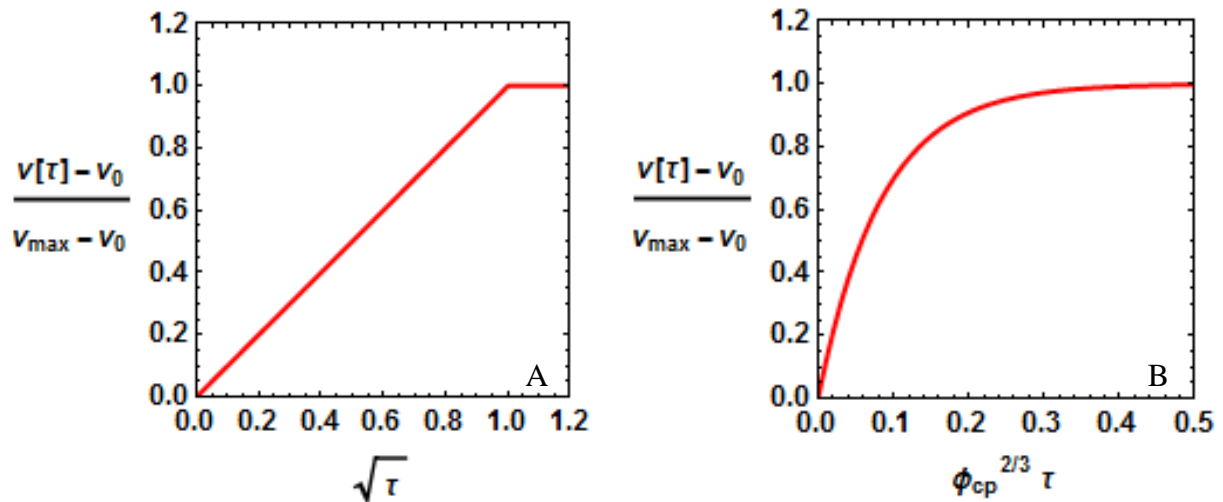


**Fig. 1** Comparison of models proposed by Hounslow et al. [14]. A. Linear growth of dimensionless granule volume as a function of the square root of time and B. Growth of dimensionless granule volume decays exponentially, scaled by  $\phi_{cp}^{2/3}$ .

Although Hounslow et al. [14] did not perform any experimental validation, Pitt et al. [18] investigated the first, static model. Experiments were conducted by nucleating granules on a

static powder bed, then extracting the granules after a set time. In this way, the growth of granules was determined as a function of time. Several systems were evaluated, with lactose and zeolite as powders and silicone oils and hydroxypropyl methylcellulose (HPMC) solutions of varying viscosities as binders. Some systems deviated from the expected trend in the early stages. Masses initially increased rapidly, after which the growth became linear with the square root of time. This behaviour was attributed to the complexity of initial wetting and nucleation effects and the short measurement times involved. In order to determine the true maximum consolidation time, an apparent final time,  $t_{max}^{app}$ , and an apparent initial volume,  $v_0^{app}$ , were introduced (Eq (5)):

$$t_{max} = t_{max}^{app} \left( \frac{v_{max} - v_0}{v_{max} - v_0^{app}} \right)^2 \quad (5)$$

Fig. 2 shows how this method employs congruence of triangles to derive the above equation; the ratio between  $v_{max}-v_0$  and  $v_{max}-v_0^{app}$  should be the same as the ratio between  $(t_{max})^{1/2}$  and  $(t_{max}^{app})^{1/2}$ .

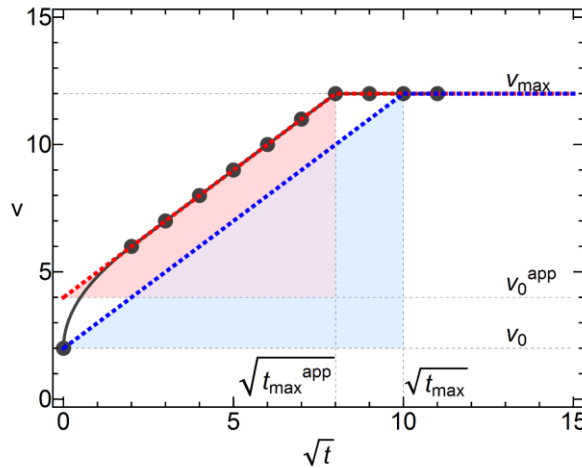


**Fig. 2** Method used by Pitt et al. [18] to convert apparent total granulation time  $t_{max}^{app}$  into the actual total granulation time  $t_{max}$  using similar triangles. Figure adapted from Pitt et al. [18].

All data fit the static model extremely well, as shown in Fig. 3. All systems investigated showed linear growth with the square root of time until  $t_{max}$ , after which no further growth occurred. However, Hounslow et al.'s method for predicting  $t_{max}$  [14], shown in Eq (2), underestimated the true growth times by several orders of magnitude. Pitt et al. [18] attributed the cause of this to significant migration of the liquid after penetration, combined with only partial saturation of the outer shell of the granules formed, as shown in Fig. 4. In the figure, an initial liquid droplet is surrounded by powder. The liquid then penetrates into the powder by capillary action. After a saturated granule is formed, the liquid proceeds to penetrate further into smaller capillaries, decreasing the saturation of the core, and incorporating air into the granule. Sun et al. investigated liquid distribution [19] and imbibition [20]. Their work has shown that a steady-state distribution is eventually reached, and confirms that air may be incorporated into the granule structure depending on the variations in pore size.

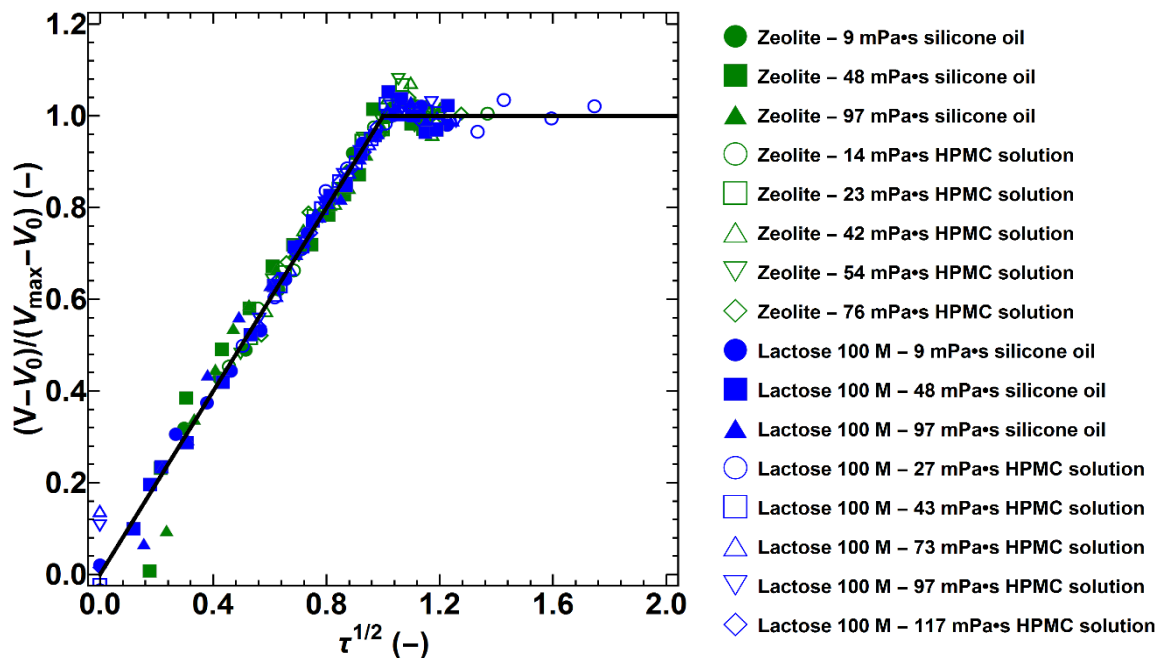
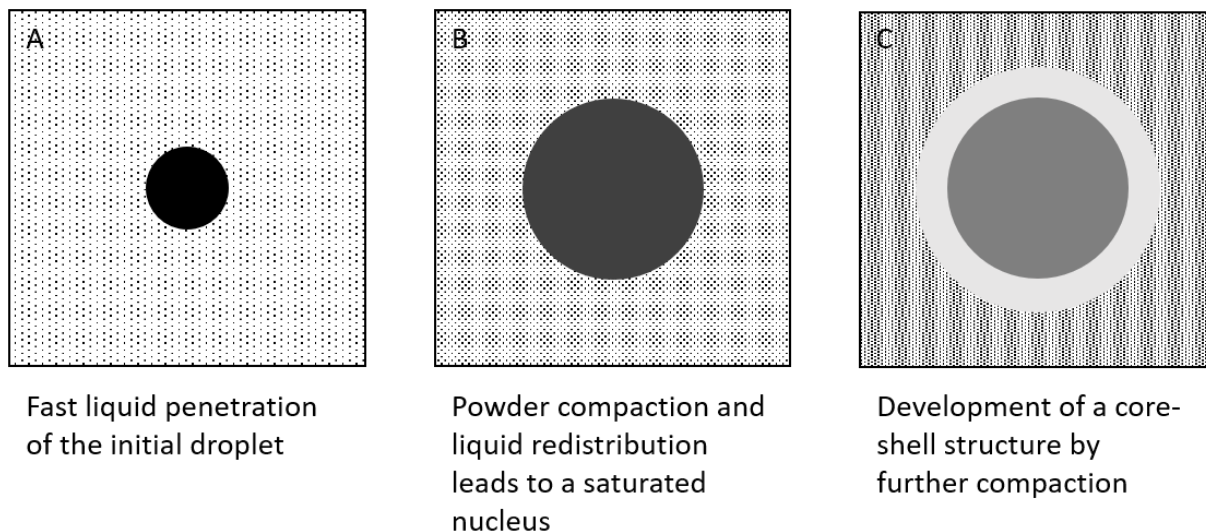


Fig. 3 All results from Pitt et al. [18] in a single plot. All data sets behave as predicted by the model, showing linear growth with the square root of time until a maximum size has been reached, after which the growth stops. Adapted from Pitt et al. [18].





**Fig. 4** The growth of a nucleus by liquid spreading and the development of a core-shell structure. Initially, the droplet (shown in A) rapidly penetrates into the powder. Through liquid spreading and impacts, the nucleus becomes a fully saturated granule (B). Further impacts cause the incorporation of air into the granule and result in a higher-density shell and lower-density core (C).

## 1.2. Scope of the paper

This current work aims to develop a mechanistic model to predict granule consolidation and layered growth and adapt this model into a growth kernel for population balance modelling (PBM). In order to achieve this, consolidation and layered growth were studied in isolation using a novel, consolidation-only granulator (COG), and the obtained experimental data was compared to models available in the literature. This paper presents the first mechanistic experimental study of consolidation and layered growth for dynamic systems, as well as the first mechanistic population balance model that describes layered growth.

## 2. Experimental

Single drop pre-nucleated granules were produced and subsequently consolidated for varying times in the newly developed consolidation-only granulator (COG). A schematic drawing of

the COG is shown in Fig. 5, and the set-up of the nucleation process in Fig. 6. The device is essentially a linear horizontal shaker, and consists of a carriage with a container moving across a straight rail. The linear motion is imparted by a flywheel with a counterweight, powered by an electrical motor. The COG was purposely designed to provide relatively gentle impacts to promote consolidation and layering while keeping breakage and attrition to a minimum. The shaker was operated at 2.5 revolutions per second, which resulted in 5 impacts per second. The peak velocity reached by the vessel was 1.6 m/s, and the Froude number corresponding to this velocity was 1.3. The overall peak force achieved was 7.4 N for lactose-based granules, and 14.8 for glass-based granules. After consolidation in the device, the granules were extracted and analysed.

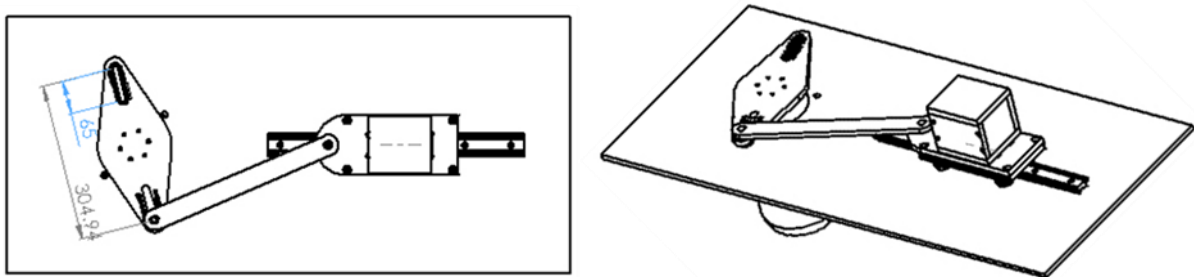


**Fig. 5** Drawing of the consolidation-only granulator using AutoCAD software. A flywheel, powered by an electrical motor, is connected to a carriage on a rail. Attached to the carriage is a detachable container that serves as the granulation vessel. Units are in mm.

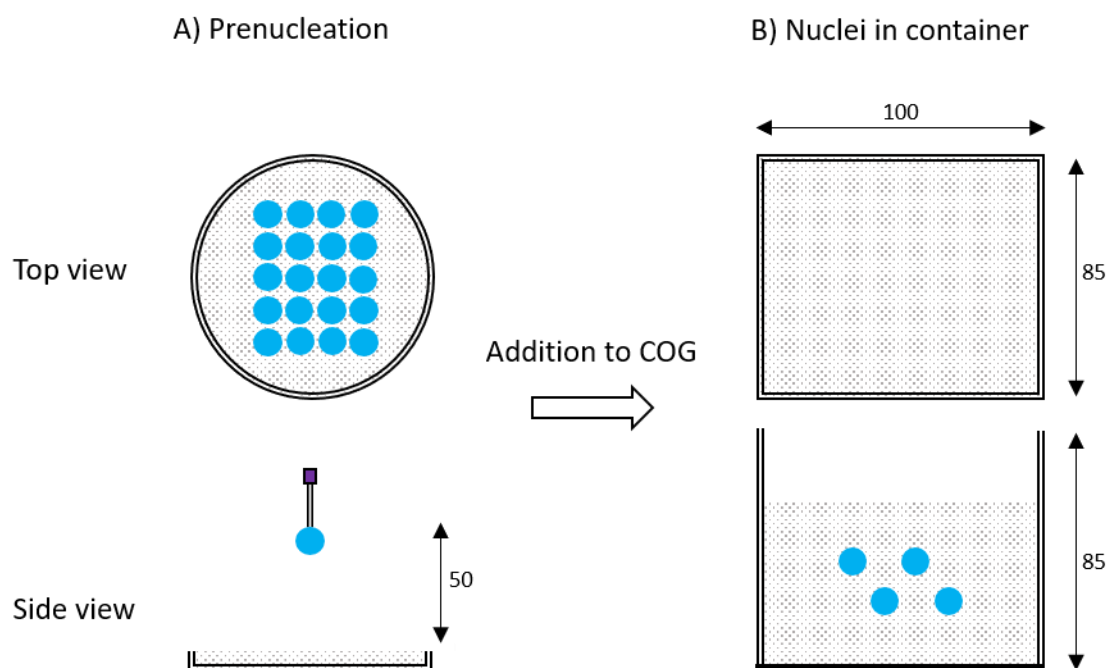


**Fig. 6** The arrangement of the granules at (A) prenucleation and (B) after addition to the container. Units are in mm.

## 2.1. Materials

Two different powders and three different binder types of varying viscosities were used for the experimental studies. For powders, crystalline lactose monohydrate (Pharmatose 100 M), referred to as *lactose* in this work and supplied by DFE Pharma, and glass beads, supplied by Mo-Sci Corporation, were selected. The properties of these powders are listed in Table 1; the particle size was obtained using dry cell laser diffraction (Malvern Mastersizer 3000 PSA), and the skeletal density was obtained using helium pycnometry (Micromeritics AccuPyc 1340). The liquid binders used were silicone oils and 50 wt% polyethylene glycol (PEG) solutions, as well as PEG 600, which has a melting point of 20-25 °C and was heated to 32.5 °C. The silicone oils and PEGs were all supplied by Sigma-Aldrich. In order to improve the visibility of the liquid binders, they were dyed. For silicone oils, Solvent Blue 59 (Sigma-Aldrich) was used. For the preparation of 50 wt% PEG solutions, a 1 wt% solution of Acid Red 1 (Sigma-Aldrich) was used. Due to the poor solubility of dyes in molten PEG, the PEG 600 binder was not dyed. The properties of the resulting binders are summarised in

Table 2; the viscosity was obtained using a rheometer (MCR502 Anton Paar Rheometer with CP50-2/TG conical plate), the surface tension was determined using image analysis of pendant droplets (First Ten Ångströms FTÅ200 goniometer with FTÅ32 software), and the density was measured using 25 mL density flasks.

**Table 1**

Powders used for the consolidation experiments and their properties. Standard errors are shown in parentheses.

<b>Powder</b>	<b>d<sub>4,3</sub> (μm)</b>	<b>Skeletal density(g/cm<sup>3</sup>)</b>
Lactose	49 (1)	1.569 (0.001)
Glass beads	74.0 (0.1)	2.496 (0.001)

**Table 2**











Binders used for the consolidation experiments and their properties. Standard errors are shown in parentheses.

<b>Binder</b>	<b>Viscosity (mPa·s)</b>	<b>Surface tension (N/m)</b>	<b>Density (g/cm<sup>3</sup>)</b>
Silicone oil 10 cSt	12.95 (0.06)	19.49 (0.07)	0.9407 (0.0001)
Silicone oil 50 cSt	51.74 (0.09)	21.11 (0.05)	0.9640 (0.0001)
Silicone oil 100 cSt	104.8 (0.1)	19.92 (0.06)	0.9684 (0.0001)
Silicone oil 1000 cSt	1042.8(0.9)	20.25 (0.08)	0.9715 (0.0001)
50 wt% PEG 4000	130 (1)	52.4 (0.6)	1.0942 (0.0001)
50 wt% PEG 20,000	3192 (9)	53.0 (0.3)	1.0953 (0.0001)
PEG 600 (32.5 °C)	94.54 (0.07)	42.9 (0.2)	1.1172 (0.0001)

Overall, ten different powder-binder systems were investigated. Throughout this work, all powder-binders systems are referred to by the liquid viscosity. A summary of these systems is shown in Table 3.

**Table 3**

All powder-binder combinations used and the symbols assigned to them in figures. Note that binders are referred to by their viscosities.

Symbol	Powder	Binder
	Lactose	13 mPa·s silicone oil
	Lactose	52 mPa·s silicone oil
	Lactose	105 mPa·s silicone oil
	Lactose	130 mPa·s PEG solution
	Lactose	3192 mPa·s PEG solution
	Lactose	95 mPa·s molten PEG
	Glass beads	52 mPa·s silicone oil
	Glass beads	105 mPa·s silicone oil
	Glass beads	1043 mPa·s silicone oil
	Glass beads	130 mPa·s PEG solution

## 2.2. Methods

The experimental procedure consisted of three steps. First, granules were pre-nucleated in a static powder bed. The nuclei were then granulated in the COG, and subsequently extracted and analysed.

### 2.2.1. Formation of pre-nucleated granules

All powder used was initially passed through a 1.18 mm sieve before use. For the experiment with molten PEG 600, the powder was heated to a temperature of 32.5 °C in order to ensure the PEG was liquid. A powder bed with an even surface was prepared in a petri dish by carefully sweeping off any excess powder using a ruler. Granules were then nucleated with a syringe pump (Harvard Apparatus PHD ULTRA) which deposited droplets from a height of 5 cm on the powder surface through a 25 Gauge (0.26 mm) tapered tip at a flow rate of 10  $\mu\text{L/s}$ . The number of granules nucleated varied between 20 and 60, depending on the expected number of undamaged granules extracted after the experiment.

### **2.2.2. Consolidation-only granulation**

To prevent the particles from sticking to the walls and bottom, the container was filled with powder for a fill level of approximately 40 %. For molten PEG 600, the container was also preheated to a temperature of 32.5 °C to prevent PEG 600 from solidifying during the granulation process. The contents of the petri dish were immediately added to the COG container after nucleation to keep static nucleation time to a minimum. After addition of the granules, a final amount of powder was added. This method prevented the wet nuclei from sticking to the lid of the container. The final fill level was controlled. In order to prevent direct impacts with the walls while ensuring the mobility of the granules, this fill level was kept constant for each powder type, which was between 50 and 75 % of the container volume. For glass beads, the total mass was 500 g, whereas the mass for lactose was 300 g.

The container was sealed and placed in the COG, which was run for a set time at 150 rpm, i.e. 5 granule impacts per second. The granules were extracted by gently passing the contents of the container through a 1.4 mm sieve, after which the individual granules were weighed using a microbalance (Mettler-Toledo XS3DU). Experiments were repeated for longer times at increasing time intervals until no change in granule mass was observed. For longer granulation times, breakage occurred despite the relatively gentle consolidation conditions provided by the COG. An experiment was deemed invalid if less than ten intact granules were extracted. Initial droplet volumes were determined by weighing individual droplets using the microbalance. In all cases, the average masses and standard deviations were calculated.

For the PEG solution-based granules, it was necessary to dry the granules before analysis. Granules were dried overnight in an oven at 32.5 °C. Granules produced from molten PEG 600-based granules were refrigerated at 5 °C instead in order for the binder to solidify.

### 2.2.3. Granule analysis

A select number of granules from each experimental data set were analysed for their true and envelope density using helium (Micromeritics AccuPyc 1340) and powder (Micromeritics GeoPyc1360) pycnometry, respectively. This selection of granules was based on the overall granulation time; the aim was to compare granules from the early stages of granulation with those from the final stages of granulation. The true density was then calculated using Eq (6).

Accurate measurement of envelope density remains a challenge for granulation researchers. In this work, the GeoPyc was used to measure the envelope volume using DryFlo powder. In this measurement technique, the DryFlo powder flows around the granules to find the volume occupied by granules. This technique has been used by other researchers (e.g. Wade et al. [21] and Rahmanian et al. [22]) to find the envelope volume of granules.

As with other porosimetry or pycnometry methods, there is some risk of ingress of the displaced medium (DryFlo powder) into the pores of the granule, which would provide a source of error in the envelope volume measurements. In this case, the DryFlo powder ( $d_{50} \sim 130\mu\text{m}$  [21]) is significantly larger than the primary particle size of the powders used in these studies (lactose  $d_{4,3} 49 \mu\text{m}$ , glass beads  $d_{4,3} 74 \mu\text{m}$ ). As a first approximation, and making the assumption that granule surface pores retain a similar pore size to the pre-nucleation powder bed, one could expect the pores in a granule formed by drop penetration and subsequent densification in the COG to be on the order of the size of the particles [10]. Given this, one would expect that some ingress of the DryFlo powder into larger pores would be possible, and this may introduce some error. However, as the DryFlo powder is significantly larger than the primary particles in the granule, it could be expected that this ingress would be relatively minor compared to the volume of the granule.

The envelope density is then calculated according to Eq (7):

$$\rho_t = \frac{m_d}{V_t} = \frac{m_p + m_b}{V_t} \quad (6)$$

$$\rho_e = \frac{m_d}{V_e} = \frac{m_p + m_b}{V_e} \quad (7)$$

Here,  $\rho_t$  is the true granule density,  $\rho_e$  is the envelope granule density,  $m_d$  is dry mass of the granule,  $m_p$  is the mass of powder in a granule,  $m_b$  is the mass of dried binder in a granule,  $V_t$  is the true or skeletal volume of a granule as measured by helium pycnometry, and  $V_e$  is the envelope volume of a granule as measured using powder pycnometry.

Additionally, X-ray tomography (Skyscan 1172 Micro-CT) was used to investigate the structural changes of two sets of granules over time: lactose-105 mPa•s silicone oil, and glass beads-105 mPa•s silicone oil. These sets were compared to the same sets produced by static nucleation where nuclei were left to grow in the petri dish without any additional granulation. Similar to the method for the density analysis, granules from early and late stages in the granulation process were selected. For each selected time, three different representative granules were evaluated, for a total of 24 images. In order to obtain the clearest images of the granules, the resolution was varied per granule, and settings were adjusted depending on the powder material. For glass beads, the pixel size varied between 4.35 and 6.44  $\mu\text{m}/\text{pixel}$ , and a voltage of 49 kV and current of 179  $\mu\text{A}$  were used. Lactose-based granules were analysed with a resolution between 4.87 and 7.83  $\mu\text{m}/\text{pixel}$ , a voltage of 40 kV and a current of 149  $\mu\text{A}$ . Images were based on a 180° scan, and a single scan was composed of 1048 images to construct a 3-D image.



### **3. Results and discussion**

In this work, both consolidation and layered growth were considered. These phenomena are discussed separately.

#### **3.1. Granule layering behaviour**

Fig. 7 presents an overview of the increase in granule mass over time for both the lactose-based and the glass beads-based systems. As expected, granule mass increases rapidly initially, and then levels off when a certain size is reached. The systems produced using silicone oils show that the time it takes to achieve the maximum size increases with increasing viscosity. However, different binders do yield different results. The systems produced with PEG solution show very little growth after an initial increase. It is possible that this short growth time is the result of drying of the binder liquid. On the other hand, the system produced with liquid PEG 600, which has a viscosity similar to that of the 105 mPa·s silicone oil, shows much more growth than any of the other systems evaluated.

Although, it was demonstrated that the granules produced in the COG display growth, determining the end points of growth proved to be difficult, since granule breakage increased with time. This phenomenon reduced the reliability of the transition between the expected growth and no-growth regime, making it difficult to obtain final granulation times and granule masses. However, since breakage does not influence the overall growth kinetics, qualitative trends obtained from data obtained at early times were assumed to be reliable.

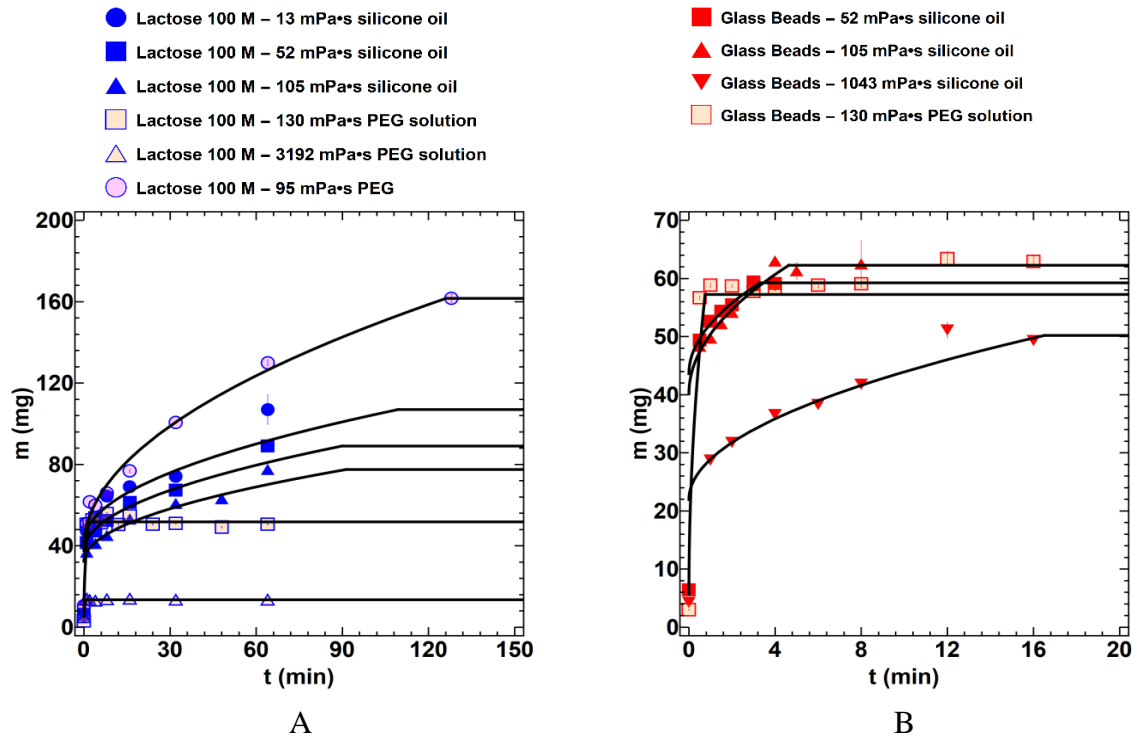


**Fig. 7** Granule mass as a function of time for (A) All lactose-based systems and (B) All glass beads-based systems. Error bars indicate standard errors.

For short granulation times, growth behaviour was found to be very reproducible, as shown in Fig. 8. At longer granulation times, growth behaviour becomes more erratic and difficult to predict. This trend is most likely caused by wear and breakage of granules, which can partially be attributed to the long times needed to achieve the maximum granule size. In addition, more extensively grown granules are larger and have a lower overall liquid content, both of which increase the possibility of breakage.

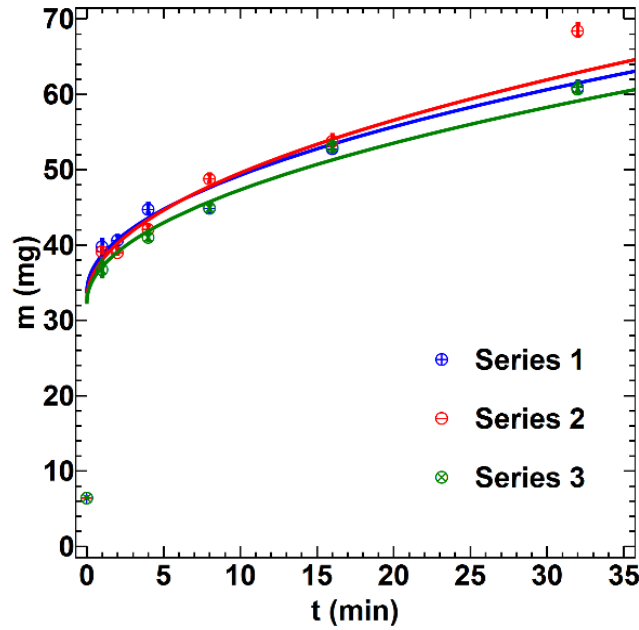


**Fig. 8** Reproducibility of granule growth for a lactose-100 cSt silicone oil system. Growth behaviour is reproducible for short granulation times.

As demonstrated, the newly designed COG is capable of reproducibly growing granules, at least for shorter granulation times. For longer granulation times, this is more difficult. However, it is possible to estimate the maximum value of the critical-packing liquid volume fraction,  $\phi_{cp}$ , by using the granule masses of the final batch with a sufficient number of intact granules. The values obtained in this way represent the lowest liquid volume fraction observed and, therefore, the greatest growth achieved. In Table 4, these estimated critical-packing liquid volume fractions are compared to critical-packing liquid volumes fractions obtained by Pitt et al. in static nucleation experiments for similar systems.

**Table 4**

Comparison of critical-packing liquid volume fractions from static experiments obtained by Pitt et al. [18] to estimated critical-packing liquid volume fractions obtained in this work by dynamic experiments.

System	$\phi_{cp,static}$ [18] (-)	$\phi_{cp,dynamic}$ (-)	Reduction (%)
Lactose-13 mPa·s silicone oil	0.217	0.087	60
Lactose-52 mPa·s silicone oil	0.204	0.112	45
Lactose-105 mPa·s silicone oil	0.196	0.134	32

For all systems, a lower critical-packing liquid volume fraction was achieved than for static systems. Clearly, the COG allows for further growth than static experiments. There are two potential causes for this difference in  $\phi_{cp}$ . In the case of growth in a static powder bed, capillary pressure and gravity are the only driving forces for consolidation and growth. In a dynamic powder bed, however, additional impact forces may allow for further consolidation, decreasing pore size and increasing liquid availability. Therefore, further and faster growth is theoretically possible. On the other hand, it is also possible that further growth occurred simply because the granule was completely surrounded by powder in a 3-D powder bed, as opposed to a '2.5-D' static powder bed, where there is no powder above the granule and where gravity might influence the liquid flow. In the former case, it is more likely that Hounslow et al.'s deformation-driven growth model applies; in the latter case, the same surface tension-driven growth model that applied to static growth is expected to apply here. It is also possible that both causes played a role in the observed difference in  $\phi_{cp}$ , in which case the dominant driving force should determine the growth kinetics.

Fig. 9 shows all experimental data fit to both Hounslow et al.'s deformation-driven growth model (A) and surface tension-driven growth model (B) [14], and all parameters used to obtain the figure are summarised in Table 5. Surprisingly, the former, dynamic model does not at all predict granule growth behaviour, whereas the latter, static model shows a good fit similar to that obtained by Pitt et al. [18]. End point behaviour is poorly predicted, however. There is a discrepancy between the predictive model and the experimental data; it appears as though some systems reach  $\phi_{cp}$  as early as  $\tau^{1/2} = 0.75$ , as shown in Fig. 9. It is unlikely that at this point, the granules would experience rapid growth, especially considering the fact that the liquid volume fraction decreases throughout the course of growth. Therefore, this discrepancy can mostly be attributed to the unreliability of the determination of the final granule mass. This issue can

20

influence the data in several ways. If attrition and breakage are prevalent at later granulation times, the maximum granule mass would increase. As a result, the data points are expected to shift down on the normalised curve, leading to a poorer fit. However, the total nucleation time will most likely also increase, which would shift all data points to the left. This could also lead to a poorer prediction, but the combined effect of these two shifts might result in a similar fit as the one shown. Therefore, it is impossible to determine the growth kinetics in this region using the current experimental data set.

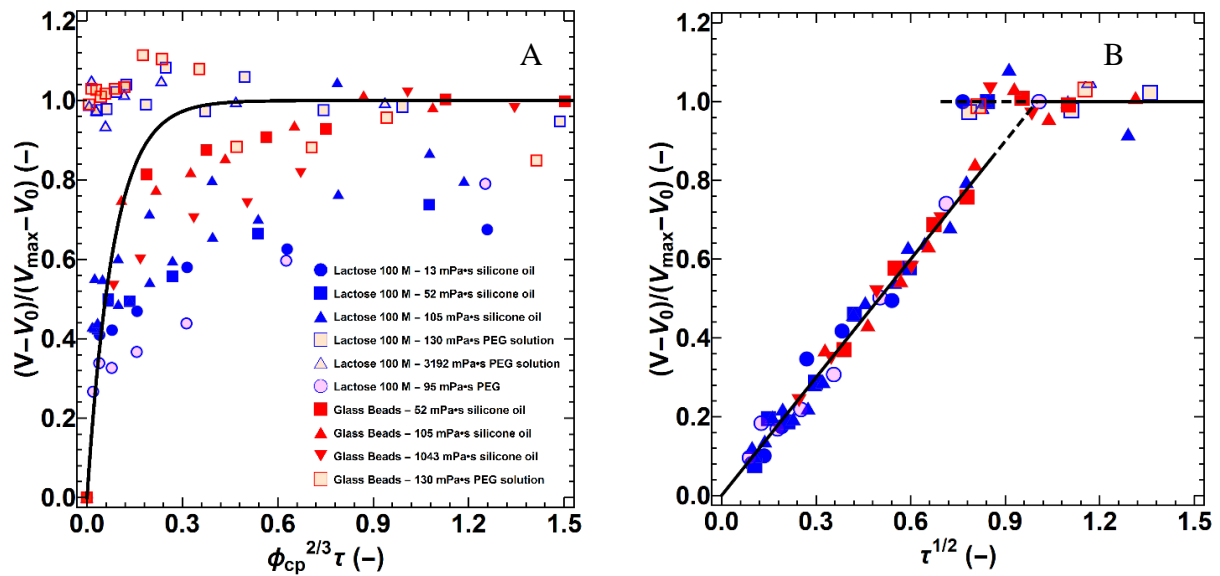


**Fig. 9** (A) All experimental data fit to the deformation-driven growth model and (B) All experimental data fit to the surface-tension driven growth model [14]. Experimental data that follows Hounslow et al.'s model for surface tension-driven growth is represented by the black line. The horizontal dashed line represents anomalous experimental data.

The poor prediction of the end points does not change the general trend observed up to  $\tau^{1/2} = 0.75$ , however, and the static model accurately predicts growth behaviour for short granulation times. Therefore, the static model appears to apply to dynamic situations as well as to static ones. This observation implies that the capillary forces are the dominant factor in granule consolidation and growth by layering.

**Table 5**

Key parameters determined from experimental data to produce Fig. 9., as well as the final saturation  $S$  of the granules.

System	$\phi_{cp}$ (-)	$D_{eff}$ (m <sup>2</sup> /s)	$t_{max}$ (min)	$S$ (-)
Lactose-13 mPa•s silicone oil	0.13	5.7E-10	226	0.31
Lactose-52 mPa•s silicone oil	0.15	5.7E-10	123	0.26
Lactose-105 mPa•s silicone oil	0.12	3.9E-10	251	0.23
Lactose-130 mPa•s PEG solution	0.23	5.0E-09	29.4	0.45
Lactose-3192 mPa•s PEG solution	0.19	1.4E-09	43.7	0.35
Lactose-95 mPa•s PEG	0.24	8.5E-09	37.6	0.19
Glass beads-52 mPa•s silicone oil	0.11	7.6E-10	232	0.32
Glass beads-105 mPa•s silicone oil	0.09	8.4E-10	264	0.31
Glass beads-1043 mPa•s silicone oil	0.20	2.9E-10	0.830	0.36
Glass beads-130 mPa•s PEG solution	0.15	6.2E-10	1.81	0.15

Table 5 also shows the final saturation values that correspond to the obtained values of  $\phi_{cp}$ . The systems lactose-105 mPa•s silicone oil, lactose-95 mPa•s PEG, and glass beads-130 mPa•s PEG solution have reached the pendular state ( $S \leq 0.25$  [23]), whereas the other systems are still in the funicular state ( $S < 0.9$  [24]). This observation implies that it is still theoretically possible for the granules to grow further, as it is still possible for liquid to drain from the liquid bridges. Consequently, the end points of growth have not yet been reached.

Compared to Pitt et al.'s work, the overall kinetics, i.e. the slope of the linear line, were found to be consistently higher when using the COG. However, the initial liquid volume used was also higher, resulting in faster growth. In order to directly compare the kinetics, Eq (8) introduces parameter  $a$ ; the slope of the growth line, divided by the initial granule volume:

$$\frac{v}{v_0} = 1 - \frac{\frac{1}{\phi_{cp}} - 1}{\sqrt{t_{max}}} \sqrt{t} = 1 - a\sqrt{t} \quad (8)$$

Table 6 compares the values of  $a$  calculated from Pitt et al.'s work [18] to the values found in this study for systems based on lactose and either silicone oil or molten PEG 600. An additional experiment was performed using Pitt et al.'s method to obtain the static values for the lactose-PEG system. From Table 6, it can be observed that for all silicone oil-based systems, Pitt et al. found a higher growth rate, although the difference appears to decrease with an increase in binder liquid viscosity. For the PEG 600-based system, the growth rate was observed to be higher in the COG. It is possible that attrition played a role in the reduction of the observed growth rate for these systems. However, a more detailed investigation is needed to validate this. For PEG 600, it is possible that exposure to air cooled the binder during growth using the static method, reducing the growth rate compared to using the COG. Overall, it appears as though the COG promotes a larger extent of growth, but does not necessarily increase the growth rate.

**Table 6**

Comparison of the slope of the growth line  $a$  for static experiments performed by Pitt et al. [18] and dynamic experiments described in this work. This study performed an additional static experiment to obtain data for 95 mPa·s liquid PEG.

<b>System</b>	<b><math>a_{static}</math> (<math>\text{min}^{-1/2}</math>)</b>	<b><math>a_{dynamic}</math> (<math>\text{min}^{-1/2}</math>)</b>
Lactose-13 mPa·s silicone oil	2.37*	0.65
Lactose-52 mPa·s silicone oil	0.82*	0.52
Lactose-105 mPa·s silicone oil	0.68*	0.47
Lactose-95 mPa·s PEG	0.31	0.73

\*calculated using data from Pitt et al. [18]

### 3.2. Granule consolidation behaviour

In order to characterise the densification of the granules, helium and powder pycnometry experiments were performed. From these experiments, the porosity of the granules was calculated. Table 7 shows the calculated porosities for the first and last set of a series of experiments that could be analysed for all experiments, as well as the relative change in porosity. Porosities were found to be relatively high, with values ranging from 0.3-0.7. The only way this

could be achieved is by the incorporation of air into the granule, since the porosity should be equal to  $\phi_{cp}$  when no air is present. This observation is in agreement with Pitt et al.'s [18] results. Furthermore, it appears as though the porosity did not change significantly between the early and late stages of granulation; in most cases, the standard error is comparable to the change in porosity, and in many cases, the porosity even increases. This is highly unexpected in a dynamic case, where consolidation is likely to occur.

**Table 7**

Granule porosities at the start and end of granulation. Standard errors are shown in parentheses.

<b>System</b>	<b><math>\epsilon_{start}</math> (-)</b>	<b><math>\epsilon_{end}</math> (-)</b>	<b>Change (%)</b>
Lactose-13 mPa•s silicone oil	0.428 (0.003)	0.408 (0.008)	-5 (2)
Lactose-52 mPa•s silicone oil	0.408 (0.007)	0.431 (0.003)	6 (2)
Lactose-105 mPa•s silicone oil	0.40 (0.06)	0.43 (0.01)	7 (15)
Lactose-130 mPa•s PEG solution	0.68 (0.01)	0.695 (0.009)	2 (2)
Lactose-3192 mPa•s PEG solution	0.37 (0.01)	0.36 (0.01)	-4 (5)
Lactose-95 mPa•s PEG	0.43 (0.04)	0.442 (0.005)	2 (2)
Glass beads-52 mPa•s silicone oil	0.490 (0.007)	0.447 (0.005)	-9 (2)
Glass beads-105 mPa•s silicone oil	0.406 (0.009)	0.433 (0.008)	7 (3)
Glass beads-1043 mPa•s silicone oil	0.39 (0.01)	0.383 (0.007)	-3 (4)
Glass beads-130 mPa•s PEG solution	0.31 (0.01)	0.342 (0.006)	12 (4)

In order to further investigate this surprising consolidation behaviour, a select number of granules were investigated using X-ray tomography and compared to statically grown granules. Images of granules from the lactose-105 mPa•s silicone oil system are shown in Fig. 10. The rings around the granules are the sample container.



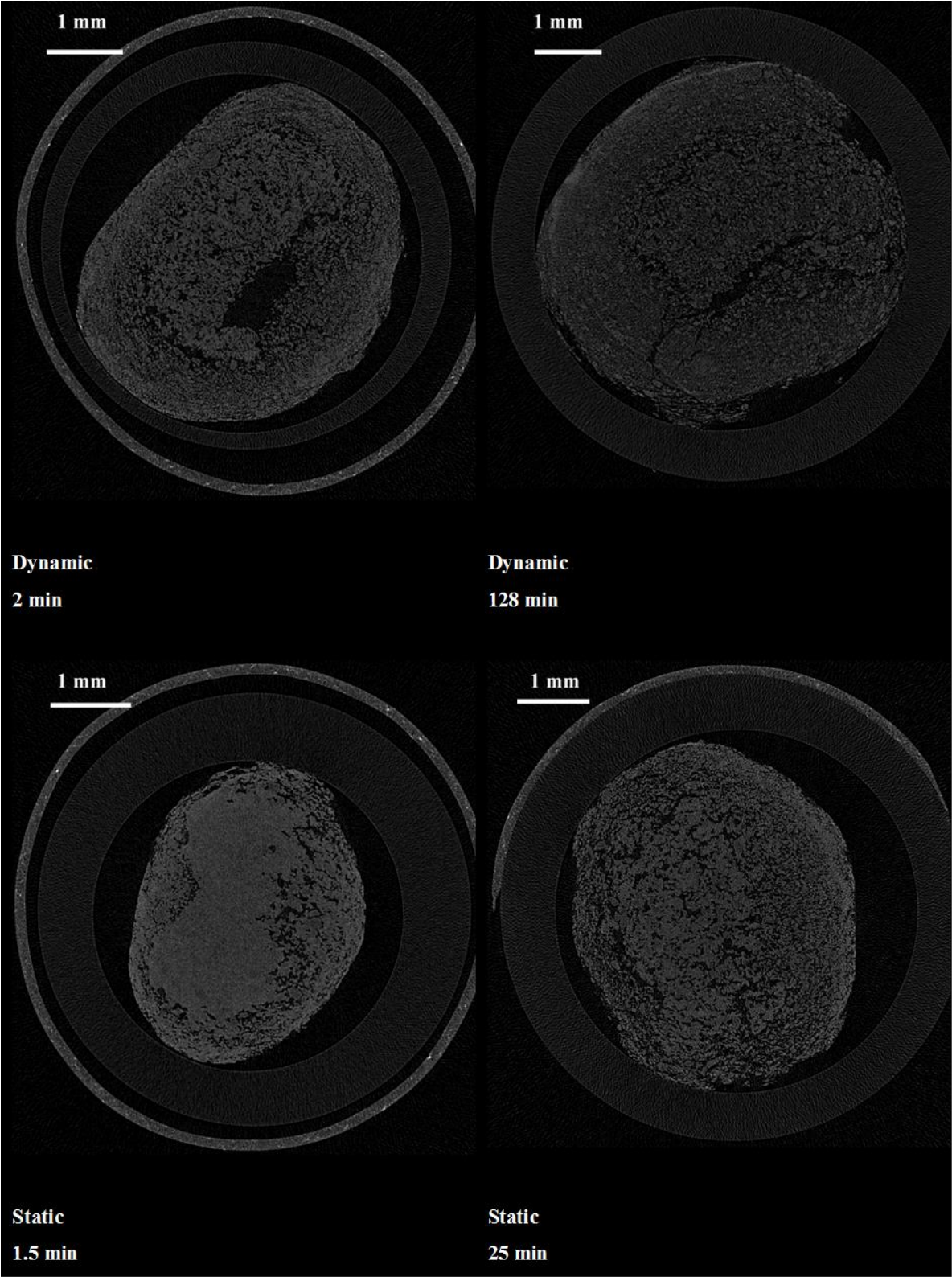


**Fig. 10** Comparison of X-ray tomography images of lactose-100 cSt silicone oil at the early and late growth times for static and dynamic situations. The rings are part of the sample container.

From Fig. 10, several observations can be made. In every image, two distinct regions can be discerned; a core and an outer shell. Since the granules were produced by drop nucleation, this is unsurprising, but there is an obvious difference between the statically and dynamically grown granules. Granules grown dynamically in the COG have a core with larger pores, represented by the black areas in the image. It is possible that the internal structure of these granules was weakened by the impacts produced by the COG. It should also be noted that these voids are already present for short granulation times. On the other hand, the cores of statically grown granules appear to be much more tightly packed, and increase in porosity over time. It is possible that this increase in porosity is caused by the movement of liquid, where voids filled with liquid drain due to capillary forces. The availability of more surface area in the 3-D situation provided by the COG might have increased liquid spreading compared to a 2.5-D static bed scenario; the non-void part of the core of the dynamically produced granule after 2 min of granulation looks very similar to the core of the statically grown granule at 25 min. There is also a clear difference in the shells of the statically and dynamically produced granules. In both scenarios, the shell thickness increases over time, but statically grown granules do not show a clear structure in the shell. Rather, the shell appears to be loosely packed around the core. For the dynamically grown granules, on the other hand, there is a clear layer-like structure to the shell. The shell layer is also much more compacted compared to the static scenario, and the increase in thickness is much more pronounced. This observation demonstrates that there is a clear consolidating effect caused by the COG. It is possible that the observed macrovoids increased the porosity determined with pycnometry measurements, leading to the unexpected consolidation trends observed in Table 7.

In conclusion, it appears as though *local* consolidation definitely occurs in the COG. However, due to the formation of macrovoids, it was found to be impossible to quantify the consolidation

behaviour using pycnometry. While X-ray tomography has been demonstrated to be valuable in determining local porosities in the shell and core, as well as the layer thickness [25-33], this did not form part of the scope of this work, and the settings chosen for the images were not conducive to this analysis.

### 3.3. Population balance modelling

Based on the experimental results, it is possible to predict layered growth using only the critical parameters  $\phi_{cp}$  and  $t_{max}$ , the latter of which is dependent on the former. In this section, the development of a growth kernel developed for population balance modelling (PBM) of a granulation process is described. In such a model, the change in number density of granules  $n$  is expressed in terms of particle size  $L$ , growth rate  $G$ , birth rate  $B$  and death rate  $D$ , as shown in Eq (9):

$$\frac{\partial n}{\partial t} + \frac{\partial (G * n)}{\partial L} = B - D \quad (9)$$

Here, the aim was to find an expression for the growth term  $G$ . In order to achieve this, the air content of the granule needs to be taken into account. In this way, the volume of the granule can be expressed in terms of its liquid content, the raw powder volume and the granule porosity. First, Eq (2) must be adapted to describe the growth of the solid volume of the granule (Eq (10)):

$$v_S = (v_{max} - v_L) * \sqrt{\frac{t}{t_{max}}} = v_L * \left(\frac{1 - \phi_{cp}}{\phi_{cp}}\right) * \sqrt{\frac{t}{t_{max}}} \quad (10)$$

where  $v_s$  is the volume of the solid powder and  $v_L$  is the volume of liquid binder. In the absence of liquid addition, this value is equal to  $v_0$ . Next, assuming a spherical granule, the diameter of the granule  $L$  can be expressed in terms of its total volume, and, by extension, in terms of its solids volume and porosity  $\varepsilon$  (Eq (11)):

$$L = \sqrt[3]{\frac{6}{\pi} * v_T} = \sqrt[3]{\frac{6}{\pi} * \frac{v_S}{1 - \varepsilon}} \quad (11)$$

Considering the growth rate  $G$  as the derivative of the granule diameter with respect to time, it is now possible to develop a term for the growth rate. First, considering a variable porosity and the possibility of liquid addition, Eq (12) may be derived:

$$\frac{dL}{dt} = \frac{\left(\frac{dv_L}{dt} * \frac{v_S}{v_L} + \frac{v_L^2}{v_S} * \left(\frac{1 - \phi_{cp}}{\phi_{cp}}\right)^2 * \frac{1}{2t_{max}}\right) * (1 - \varepsilon) + v_S * \frac{d\varepsilon}{dt}}{\frac{\pi}{2} * (1 - \varepsilon)^2 * \sqrt[3]{\left(\frac{6}{\pi} * \frac{v_S}{1 - \varepsilon}\right)^2}} \quad (12)$$

Here, the first term in the numerator describes changes in the surface-tension driven growth rate due to addition or evaporation of liquid. The second term describes regular surface tension-driven growth, and the third term the change in the growth rate by consolidation. Since this work was not able to quantify consolidation, the overall consolidation was considered constant, eliminating this term. Further simplification can be performed by assuming no liquid

evaporation or addition, as was the case for the silicone oil-based experiments in this work.

Applying these simplifications yields a straightforward expression for  $G$  (Eq (13)):

$$G = \frac{\frac{v_L^2}{v_S} * \left(\frac{1 - \phi_{cp}}{\phi_{cp}}\right)^2 * \frac{1}{2 t_{max}}}{\frac{\pi}{2} * (1 - \varepsilon) * \sqrt[3]{\left(\frac{6}{\pi} * \frac{v_S}{1 - \varepsilon}\right)^2}} \quad (13)$$

However, since a granule may start out as a liquid drop (with an infinite local porosity) surrounded by powder, this expression is not valid over the whole range of possible values for  $v_S$ . There is a *critical granule volume*,  $v_{crit}$ , below which the granule contains a portion of the original liquid drop, undistributed through the granule. Assuming that there is no air incorporated into this nucleus granule, the critical granule volume can be defined according to Eq (14):

$$v_{crit} = v_L \frac{1 - \varepsilon}{\varepsilon} \quad (14)$$

Here,  $\varepsilon$  is the porosity at the moment before air is incorporated. At this point, the total granule volume  $v_T$  is defined as the sum of  $v_S$  and  $v_L$ .

Finally, the no-growth regime can simply be defined as the point where the liquid volume fraction in absence of air is greater than the critical-packing liquid volume fraction. The three regimes identified can then be defined as in Eq (15):

$$G = \begin{cases} \frac{v_L^2}{v_S} * \left(\frac{1 - \phi_{cp}}{\phi_{cp}}\right)^2 * \frac{1}{2 t_{max}} & v_S < v_{crit} \\ \frac{\pi}{2} * \sqrt[3]{\left(\frac{6}{\pi} * (v_S + v_L)\right)^2} & \\ \frac{v_L^2}{v_S} * \left(\frac{1 - \phi_{cp}}{\phi_{cp}}\right)^2 * \frac{1}{2 t_{max}} & \frac{v_L}{v_L + v_S} > \phi_{cp} \\ \frac{\pi}{2} * (1 - \varepsilon) * \sqrt[3]{\left(\frac{6}{\pi} * \frac{v_S}{1 - \varepsilon}\right)^2} & \\ 0 & \frac{v_L}{v_L + v_S} \leq \phi_{cp} \end{cases} \quad (15)$$

Here, the first regime is the regime where the granule contains a portion of the undistributed initial drop, the second regime is the regime where growth occurs with incorporation of air into the granule and the final regime is the no-growth regime. The model developed here differs from the widely used model developed by Cameron et al. [11] in its mechanistic basis, with easily obtainable parameters that are system-dependent. However, the growth rate is independent of the available amount of powder in the granulator. This could be a problem for the solution of the equations, but a mass balance should resolve this issue.

To evaluate this expression for the growth term, a population balance model was considered with only layered growth, as shown in Eq (16):

$$\frac{\partial n}{\partial t} + \frac{\partial (G * n)}{\partial L} = 0 \quad (16)$$

In order to solve the population balance equations, they were discretised according to standard discretisation [34]. This method is known to overpredict the moments, but it suffices for a

simple demonstration of the potential applications of this kernel. The discretised set of equations is shown in Eq (17):

$$G_i = \begin{cases} \frac{v_L^2 * \left(\frac{1 - \phi_{cp}}{\phi_{cp}}\right)^2 * \frac{1}{2 t_{max}}}{\frac{\pi}{2} * (L_i + d_p)^2 * \left(\left(\frac{\pi}{6} * (L_i + d_p)^3\right) - v_L\right)} & i = 1 \\ \frac{v_L^2 * \left(\frac{1 - \phi_{cp}}{\phi_{cp}}\right)^2 * \frac{1}{2 t_{max}}}{\frac{\pi}{2} * L_i^2 * \left(\left(\frac{\pi}{6} * L_i^3\right) - v_L\right)} & \left(\frac{\pi}{6} * L_i^3\right) - v_L < v_{crit} \\ \frac{v_L^2 * \left(\frac{1 - \phi_{cp}}{\phi_{cp}}\right)^2 * \frac{1}{2 t_{max}}}{\frac{\pi^2}{12} * (1 - \varepsilon)^2 * L_i^5} & \frac{v_L}{v_L + \left((1 - \varepsilon) * \frac{\pi}{6} * L_i^3\right)} > \phi_{cp} \\ 0 & \frac{v_L}{v_L + \left((1 - \varepsilon) * \frac{\pi}{6} * L_i^3\right)} \leq \phi_{cp} \end{cases} \quad (17)$$

It should be noted that for the lowest bin size ( $i = 1$ ), the granule size was assumed to be equal to the liquid droplet size and a single powder layer. This assumption was made to prevent the initial growth term from being infinite. Implementation of this kernel was performed for a layered growth-only simulation at several bin size ratios,  $r$ . For the values of  $\phi_{cp}$ ,  $t_{max}$ ,  $v_L$  and  $\varepsilon$ , the experimental values from the lactose-105 mPa\*s silicone oil system were used. The obtained curves were compared to the experimental data of the same set, as well as the fit to the data. The results are shown in Fig. 11.

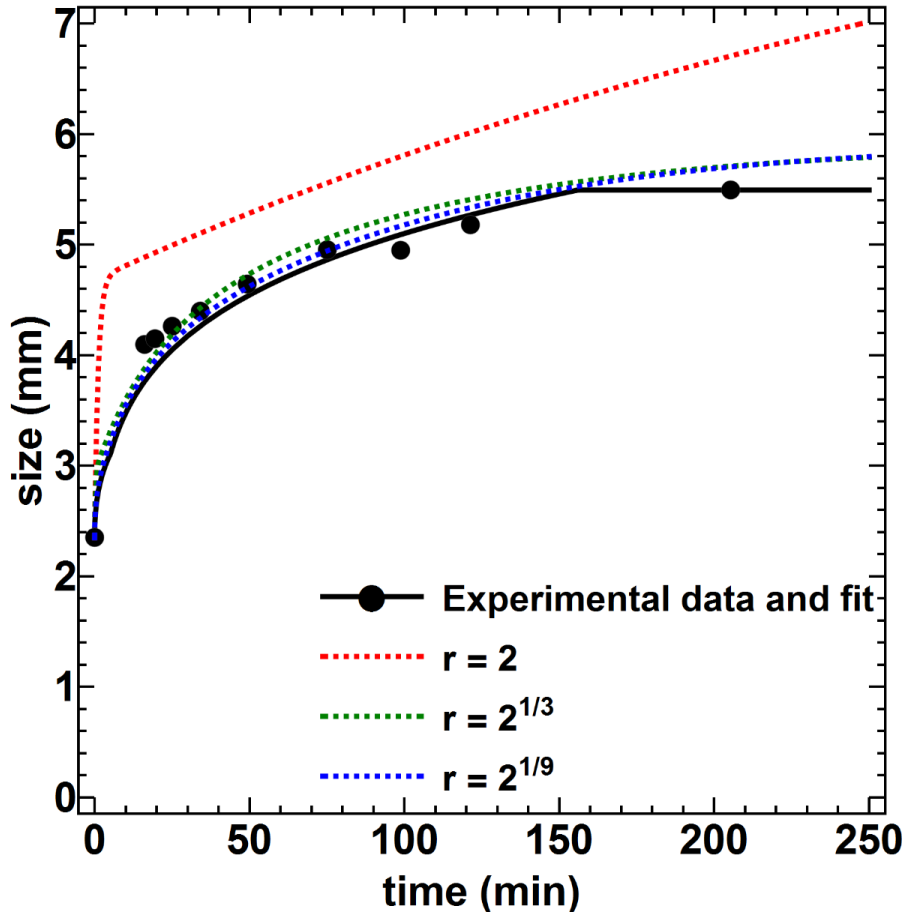


**Fig. 11** Comparison of particle size as a function of time for both the experimental and simulated data at various values of bin size ratio  $r$ .

Unsurprisingly, a bin size ratio of 2 does not accurately reflect granule growth at all. However, a value of  $2^{1/3}$  shows good agreement with the experimental results, and this can be further improved by reducing the bin size to  $2^{1/9}$ . Fig. 11 also clearly shows the limitation of discretisation; since discretisation divides granules into size classes, there is a tendency to overestimate the final granule size. However, different solution methods may yield better results. The layering kernel developed here has been designed specifically with integration with other population balance kernels in mind, and the relatively small bin size ratio of  $2^{1/3}$  demonstrates that this kernel can be combined with other equations. In this way, the development is a valuable



contribution for the modelling of more complex granulation processes that include breakage, attrition, agglomeration and nucleation in addition to layered growth. The ability to include all rate processes in the simulation of granulation should enable industry to design better granulation processes and granulated products.

## **4. Conclusions**

In this work, a novel consolidation-only granulator (COG) was developed and used to understand the of consolidation and layering kinetics of pre-nucleated granules. For the first time, a model for the kinetics of dynamic layered growth was experimentally validated. Additionally, a mechanistically based population balance model kernel for layered granule growth has been developed. This is the first mechanistically-based population balance kernel for layered growth, and represents a significant advancement in the field.

It was found that the COG, which is based on a linear shaker, was capable of densifying granules. Although the experiments performed were dynamic, the kinetics were found to agree with the static growth model proposed by Hounslow et al. [14]. This model, which was experimentally validated by Pitt et al. [18], is based on surface tension-driven flow, and predicts linear increase of granule volume with the square root of time. The kinetics were predicted by the static model, but the results show that the extent of granule growth was larger for the dynamic method compared to static nucleation. Porosity measurements suggested that no overall consolidation occurred. However, further investigation using X-ray tomography revealed that granules displayed a core-shell structure, with the core being less dense than the shell, and the shell increasing in thickness as granulation progressed. The population balance model developed in

this work shows promising results, agreeing well with experimental data. Furthermore, the model allows for easy expansion to include more complex phenomena.

The results of this work offer a significant further insight into the consolidation and layered growth mechanism. Despite this, several questions remain to be answered for these kinetics to be fully mapped or predicted. Currently, the final granulation times and associated critical-packing liquid volume fractions are determined experimentally, and are equipment and method-dependent. A predictive method to determine these values would be very beneficial. Additionally, combining the growth kernel from this work with other rate process kernels, and comparing the results to experimental granulation data would allow for the evaluation of the performance of the model under such conditions.

To conclude, this work has shown that it is possible to separate consolidation and layered growth from the other granulation mechanisms, has validated a model of the kinetics of granule growth by layering, and has successfully proposed a mechanistic kernel for population balance modelling. These findings pave the way to better design and control of granulation processes.

## List of symbols

Symbol	Definition	SI units
$a$	Slope of the growth line	$(1/s^{1/2})$
$B$	Granule birth rate	$(1/s \cdot m^3)$
$D$	Granule death rate	$(1/s \cdot m^3)$
$d_{4,3}$	De Brouckere mean diameter	(m)
$d_{50}$	Median particle size	(m)
$D_{eff}$	Effective diffusion coefficient	$(m^2/s)$
$d_p$	Particle size	(m)
$G$	Granule growth rate	$(1/s \cdot m^2)$
$G$	Maximum granule growth rate	$(1/s \cdot m^2)$

$h_0$	Initial granule size	(m)
$i$	Bin number	(-)
$k$	Fitting parameter 1 in Cameron et al.'s model [11]	(-)
$L$	Granule size	(m)
$M_i$	Mass of fine powder	(kg)
$M_{powder}$	Mass of particles in size class $i$	(kg)
$m$	Granule mass	(kg)
$m_b$	Dry binder mass	(kg)
$m_d$	Dry granule mass	(kg)
$m_p$	Powder mass	(kg)
$n$	Number density of granules	(1/m <sup>3</sup> )
$S$	Saturation	(-)
$t$	Time	(s)
$t_{max}$	Total nucleation time	(s)
$t_{max}^{app}$	Apparent total nucleation time	(s)
$v$	Granule volume	(m <sup>3</sup> )
$v_0$	Initial granule volume	(m <sup>3</sup> )
$v_0^{app}$	Apparent initial granule volume	(m <sup>3</sup> )
$v_{Crit}$	Critical granule volume	(m <sup>3</sup> )
$V_e$	Envelope volume as measured using powder pycnometry	(m <sup>3</sup> )
$v_L$	Granule liquid volume	(m <sup>3</sup> )
$v_{max}$	Final granule volume	(m <sup>3</sup> )
$v_S$	Granule solid volume	(m <sup>3</sup> )
$V_t$	True volume as measured using helium pycnometry	(m <sup>3</sup> )
$v_T$	Total granule volume	(m <sup>3</sup> )
$x_w$	Moisture content	(-)
$x_w$	Critical moisture content	(-)
$\alpha$	Fitting parameter 2 in Cameron et al.'s model [11]	(-)
$\gamma$	Adhesive tension	(N/m)
$\varepsilon$	Granule porosity	(-)
$\mu$	Viscosity	(Pa·s)
$\rho$	Liquid density	(kg/m <sup>3</sup> )
$P_e$	Envelope density	(kg/m <sup>3</sup> )
$\rho_s$	True density	(kg/m <sup>3</sup> )
$\tau$	Dimensionless time	(-)
$\phi$	Liquid volume fraction	(-)
$\phi_{cp}$	Critical-packing liquid volume fraction	(-)

## Acknowledgements

The authors wish to acknowledge financial support from the EPSRC (EP/K02566X/1).

## References

- [1] K. Hapgood, M. Rhodes, Size Enlargement, in: M. Rhodes, Editor, Introduction to Particle Technology, John Wiley & Sons Ltd., Chichester, 2008, pp. 337-358.
- [2] J. Litster, B.J. Ennis, L. Liu, The Science and Engineering of Granulation Processes, Kluwer Academic Publishers, Dordrecht, 2004.
- [3] S.M. Iveson, J.D. Litster, K. Hapgood, B.J. Ennis, Nucleation, growth and breakage phenomena in agitated wet granulation processes: a review, Powder Technol. 117 (2001) 3-39.
- [4] A.D. Salman, G.K. Reynolds, H.S. Tan, I. Gabbott, M.J. Hounslow, Breakage in granulation, in: A.D. Salman, M.J. Hounslow, and J.P.K. Seville, Editors, Handbook of Powder Technology, Elsevier Science B.V., 2007, pp. 979-1040.
- [5] R. Gokhale, Y. Sun, A.J. Shukla, High-shear granulation, in: D.M. Parikh, Editor, Handbook of Pharmaceutical Granulation Theory, Taylor & Francis Group, LLC, Boca Raton, 2005, pp. 191-228.
- [6] K.P. Hapgood, J.D. Litster, R. Smith, Nucleation regime map for liquid bound granules, AIChE J. 49 (2003) 350-361.
- [7] S.M. Iveson, J.D. Litster, Growth regime map for liquid-bound granules, AIChE J. 44 (1998) 1510-1518.
- [8] S.M. Iveson, P.A.L. Wauters, S. Forrest, J.D. Litster, G.M.H. Meesters, B. Scarlett, Growth regime map for liquid-bound granules: further development and experimental validation, Powder Technol. 117 (2001) 83-97.
- [9] J.D. Litster, K.P. Hapgood, J.N. Michaels, A. Sims, M. Roberts, S.K. Kameneni, T. Hsu, Liquid distribution in wet granulation: dimensionless spray flux, Powder Technol. 114 (2001) 32-39.
- [10] K.P. Hapgood, J.D. Litster, S.R. Biggs, T. Howes, Drop penetration into porous powder beds, J. Colloid Interf. Sci. 253 (2002) 353-366.
- [11] I.T. Cameron, F.Y. Wang, C.D. Immanuel, F. Stepanek, Process systems modelling and applications in granulation: a review, Chem. Eng. Sci. 60 (2005) 3723-3750.
- [12] F.Y. Wang, X.Y. Ge, N. Balliu, I.T. Cameron, Optimal control and operation of drum granulation processes, Chem. Eng. Sci. 61 (2006) 257-267.
- [13] F.Y. Wang, I.T. Cameron, A multi-form modelling approach to the dynamics and control of drum granulation processes, Powder Technol. 179 (2007) 2-11.
- [14] M.J. Hounslow, M. Oullion, G.K. Reynolds, Kinetic models for granule nucleation by the immersion mechanism, Powder Technol. 189 (2009) 177-189.

- [15] K. Terrazas-Velarde, M. Peglow, E. Tsotsas, Investigation of the kinetics of fluidized bed spray agglomeration based on stochastic methods, *57* (2011) 3012-3026.
- [16] K. Terrazas-Velarde, M. Peglow, E. Tsotsas, Kinetics of fluidized bed spray agglomeration for compact and porous particles, *Chem. Eng. Sci.* *66* (2011) 1866-1878.
- [17] R. Maxim, J.S. Fu, M. Pickles, A. Salman, M. Hounslow, Modelling effects of processing parameters on granule porosity in high-shear granulation, *Granul. Matter* *6* (2004) 131-135.
- [18] K. Pitt, R.M. Smith, S.A.L. de Koster, J.D. Litster, M.J. Hounslow, Kinetics of immersion nucleation driven by surface tension, *Powder Technol.* *335* (2018) 62-69.
- [19] Y. Sun, A. Kharaghani, T. Metzger, J. Müller, E. Tsotsas, Lotion distribution in wet wipes investigated by pore network simulation and X-ray micro tomography, *Transport Porous Med.* *107* (2015) 449-468.
- [20] Y. Sun, A. Kharaghani, E. Tsotsas, Micro-model experiments and pore network simulations of liquid imbibition in porous media, *Chem. Eng. Sci.* *150* (2016) 41-53.
- [21] J.B. Wade, G.P. Martin, D.F. Long, Controlling granule size through breakage in a novel reverse-phase wet granulation process; the effect of impeller speed and binder liquid viscosity, *Int. J. Pharm.* *478* (2015) 439-446.
- [22] N. Rahmanian, A. Najji, M. Ghadiri, Effects of process parameters on granules properties produced in a high shear granulator, *Chemical Engineering Research & Design* *89* (2011) 512-518.
- [23] A.F. Blandin, D. Mangin, C. Subero-Couroyer, A. Rivoire, J.P. Klein, J.M. Bossoutrot, Modelling of agglomeration in suspension: Application to salicylic acid microparticles, *Powder Technology* *156* (2005) 19-33.
- [24] P. Pierrat, H.S. Caram, Tensile strength of wet granula materials, *Powder Technol.* *91* (1997) 83-93.
- [25] C.S. Omar, R.M. Dhenge, J.D. Osborne, T.O. Althaus, S. Palzer, M.J. Hounslow, A.D. Salman, Roller compaction: effect of morphology and amorphous content of lactose powder on product quality, *Int. J. Pharm.* *496* (2015) 63-74.
- [26] R.B. Al-Asady, R.M. Dhenge, M.J. Hounslow, A.D. Salman, Roller compactor: determining the nip angle and powder compaction progress by indentation of the pre-compacted body, *Powder Technol.* *300* (2016) 107-119.
- [27] N.B. Davis, K. Waibel, K. Wang, J.D. Litster, Microstructure of single-droplet granules formed from ultra-fine powders, *Powder Technol.* *305* (2017) 19-26.
- [28] A.Z. Al hassn, S. Jeßberger, M.J. Hounslow, A.D. Salman, Multi-stage granulation: an approach to enhance final granule attributes, *Chem. Eng. Res. Des.* *134* (2018) 26-35.
- [29] B. Khorsheed, I. Gabbott, G.K. Reynolds, S.C. Taylor, R.J. Roberts, A.D. Salman, Twin-screw granulation: understanding the mechanical properties from powder to tablets, *Powder Technol.* *314* (2019) 105-155.
- [30] A.D. Rajkumar, G.K. Reynolds, D. Wilson, S.A.C. Wren, A.D. Salman, The effect of roller compaction and tableting stresses on pharmaceutical tablet performance, *Powder Technol.* *341* (2019) 23-37.
- [31] M. Dadkhah, M. Peglow, E. Tsotsas, Characterization of the internal morphology of agglomerates produced in a spray fluidized bed by X-ray tomography, *Powder Technol.* *228* (2012) 349-358.
- [32] C. Rieck, T. Hoffmann, A. Bück, M. Peglow, E. Tsotsas, Influence of drying conditions on layer porosity in fluidized bed spray granulation, *Powder Technol.* *272* (2015) 120-131.

- [33] F. Sondej, A. Bück, K. Koslowsky, P. Bachmann, M. Jacob, E. Tsotsas, Investigation of coating layer morphology by micro-computed X-ray tomography, *Powder Technol.* 273 (2015) 165-175.
- [34] M.J. Hounslow, R.L. Ryall, V.R. Marshall, A discretized population balance for nucleation, growth, and aggregation, *AICHE J.* 34 (1988) 1821-1832.